# Rippling mode in the subsolar magnetopause current layer and its influence on three-dimensional magnetic reconnection

P. L. Pritchett[1] and F. S. Mozer[2]

Received 6 October 2010; revised 22 December 2010; accepted 8 February 2011; published 19 April 2011.

[1] The properties of an asymmetric magnetopause current layer without a guide magnetic field are investigated using three-dimensional particle-in-cell simulations. The low-density (magnetosphere) side of the current layer is found to be unstable to an internal mode that ripples the current layer with a wavelength comparable to the ion inertia length based on the high (magnetosheath) density. These modes produce localized perpendicular electric fields with peak magnitude of the order of 100 mV/m, which is more than an order of magnitude greater than in corresponding two-dimensional treatments. The rippling of the current sheet leads to a modulation in the east-west direction on time scales of the order of a second of the electron outflows and Poynting flux produced by magnetic reconnection.

**Citation:** Pritchett, P. L., and F. S. Mozer (2011), Rippling mode in the subsolar magnetopause current layer and its influence on three-dimensional magnetic reconnection, *J. Geophys. Res.*, *116*, A04215, doi:10.1029/2010JA016190.

## 1. Introduction

[2] The overwhelming majority of theoretical analyses and simulations of collisionless magnetic reconnection in the magnetosphere have dealt with 2-D configurations in which the plasma density and the magnitude of the reconnecting component of the magnetic field are similar on the two sides of the current sheet. While such a symmetric 2-D approach has been quite successful in establishing the basic principles of collisionless reconnection [e.g., *Birn and Priest*, 2007, chapter 3], it is clearly not adequate to deal with reconnection at the subsolar magnetopause. Out of more than 120 subsolar magnetopause crossings studied by *Mozer et al.* [2002] and *Mozer and Retinò* [2007], only one exhibited the characteristic features of the simple 2-D symmetric reconnection model without a guide field. In addition, there have been suggestions that 3-D effects could be especially important in magnetopause reconnection where the overlap of multiple tearing modes growing on different magnetic surfaces could cause field lines inside the magnetopause current layer to be stochastic [*Galeev et al.*, 1986] or where the fastest growing tearing instability could occur for oblique angles in the presence of a moderate guide field [*Daughton and Karimabadi*, 2005].

[3] A number of 2-D simulation studies have included one or more of the asymmetric effects associated with unequal asymptotic magnetic field strengths and gradients in density and temperature across the magnetopause current layer [*Ding et al.*, 1992; *Swisdak et al.*, 2003; *Pritchett*, 2008; *Tanaka et al.*, 2008; *Huang et al.*, 2008; *Pritchett and Mozer*, 2009], and these asymmetric treatments have produced agreement with many of the observed features of subsolar reconnection [*Mozer et al.*, 2008; *Tanaka et al.*, 2008; *Mozer and Pritchett*, 2009]. A recent analysis of Polar data [*Mozer and Pritchett*, 2010], however, has identified an apparent discrepancy between the magnetopause observations and the asymmetric simulations. Burst data from the electric field experiment on the Polar spacecraft were examined when the spacecraft was on the dayside of the Earth and the apogee of 9.5 $R_E$ was near the equator. Seventeen events were found at reconnecting magnetopauses with perpendicular electric field components as large as 200 mV/m and parallel electric field components as large as 80 mV/m. The full width at half maximum for these events ranged from less than 0.2 to 15 ms. The parallel electric fields were associated with significant plasma density depletions, and they all appeared on the magnetospheric side of the current sheet. Such large parallel electric fields are 1–2 orders of magnitude stronger than observed in the 2-D simulations, and their anticorrelations with plasma density were also not found in the simulations.

[4] In the present note we report the results of particle-in-cell (PIC) simulations of asymmetric reconnection without a guide field in full 3-D. These simulations show that the magnetospheric side of the magnetopause is unstable to an internal mode that ripples the current layer in the east-west direction. The wavelength of the mode is of the order of 200 km, and it produces localized perpendicular electric fields with peak magnitudes of the order of 100 mV/m. However, the effects of the rippling of the current sheet on magnetic reconnection appear to be relatively minor away from the immediate X line region. There is a modulation of

[1]Department of Physics and Astronomy, University of California, Los Angeles, California, USA.
[2]Space Sciences Laboratory, University of California, Berkeley, California, USA.


0148-0227/11/2010JA016190

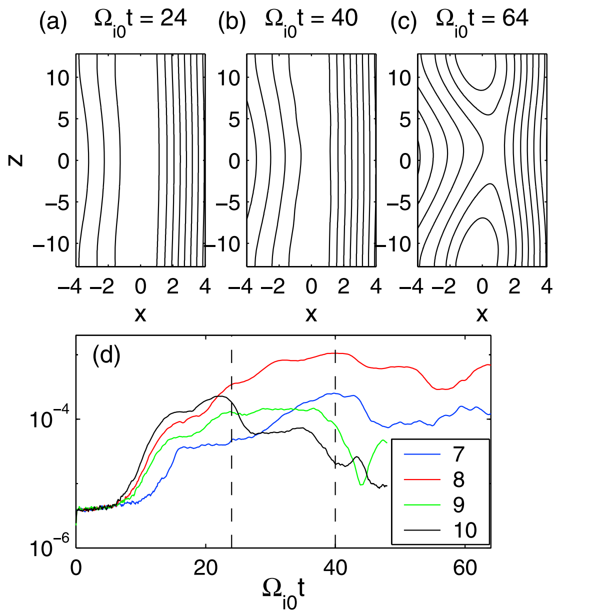


**Figure 1.** Time development of the 3-D asymmetric magnetic reconnection simulation. (a–c) Magnetic field lines in the $x,z$ plane averaged over all $y$ at times $\Omega_{i0}t$ = 24, 40, and 64; (d) time history of the amplitude squared for the $k_y$ = 7, 8, 9, and 10 density modes averaged over $x$ and $z$. The dashed vertical lines in Figure 1d indicate the times corresponding to the field line plots in Figures 1a and 1b.

the electron outflows and Poynting flux on time scales of the order of a second, but this is a factor of 100 times longer than the bursts observed by Polar. Also, the parallel electric fields accompanying the modulation are significantly smaller than those seen by Polar.

## 2. Simulation Model

[5] The initial asymmetric current sheet configuration is the same as used in our previous 2-D simulations of asymmetric reconnection [*Pritchett*, 2008; *Pritchett and Mozer*, 2009]. The reversing magnetic field $B_z(x)$ changes from $-0.5B_0$ on the magnetosheath side to $1.5B_0$ on the magnetosphere side, and the density drops from $n_0$ on the sheath side to $0.1n_0$ on the sphere side. The spatial grid is now 3-D, with grid dimensions $N_x \times N_y \times N_z = 512 \times 256 \times 512$. Periodic boundary conditions are used in the $y$ direction. To compensate for the extra cost of the 3-D simulation, the ion to electron mass ratio is reduced to $m_i/m_e = 50$ as compared to the value of 200 used in the 2-D simulations. The ion inertia length $d_i = c/\omega_{pi}$ based on the density $n_0$ is $d_i = 20\Delta$, where $\Delta$ is the grid spacing, and the speed of light is $c/v_A = 10$, where the Alfvén speed $v_A = B_0/(4\pi n_0 m_i)^{1/2}$. The initial current sheet half-thickness is $\lambda = d_i$, and the temperature ratio is $T_i/T_e = 2$. The total number of particles used in the simulation is 7.0 billion, corresponding to a reference density $n_0$ of 83 particles per species per cell. The initial guide field is set to zero in the present simulation, and the simulation is driven by applying a localized convection field $E_{0y}(z)$ at the magnetosheath $x$ boundary as given in the work by *Pritchett and Mozer* [2009]. In the coordinate system used in the simulations, $x$ is directed from the magnetosheath side toward the magnetosphere side of the current layer, $y$ is directed dawnward, and $z$ is directed northward.

## 3. Simulation Results

### 3.1. Rippling of the Current Sheet

[6] The early stage of the 3-D simulation is dominated by the growth of a number of finite $k_y$ modes that have the effect of rippling the current sheet. These modes grow and saturate before there is significant reconnection (Figure 1). The growth of the modes is concentrated in modes 7 to 14, with mode 10 dominating initially (Figure 1d). Its linear growth rate is $\gamma/\Omega_{i0} \approx 0.2$. By $\Omega_{i0}t \approx 24$, however, mode 8 has become dominant, and this dominance persists during the rest of the simulation.

[7] Figure 2 shows the structure in the equatorial plane ($z = 0$) at time $\Omega_{i0}t = 40$ of (a) the density, (b) the magnetic field $B_z$ (with the electron bulk flow velocity shown by black arrows), (c) the electric field $E_x$, and (d) the electric field $E_y$. There is a very clear excitation of mode 8 on the magnetosphere side of the current layer for $1.2 < x/d_i < 2.5$. At this time, the null in $B_z$ is at $x/d_i \approx 0.4$. Based on the average initial field in this region of $B_z = 1.4\ B_0$, the electron gyroradius is $\rho_e = 1.7\Delta$, and the wave number of mode 8 is $k_y\rho_e = 0.34$ ($k_y\rho_i = 3.4$). The adiabaticity parameter [*Büchner and Zelenyi*, 1987] $\kappa_e = (B_{0z}/B_0)(\lambda/\rho_e)^{1/2} = 4.8$, indicating that the electrons are well magnetized. From Figure 2b it is clear that the electron flow is frozen-in to the magnetic field and follows the ripples in the field. This flow arises from the $E_{x,y} \times B_z$ drift. The ripples in the density and $B_z$ are in phase with each other, while the extrema in $E_y$ are 90° out of phase as expected since they drive the electron $x$ flows. The peak value of the electron flow is $2.8v_A$ and occurs in a region where $B_z \approx 0.8B_0$. In contrast, the ion flow is relatively unaffected by the rippling modes, with the peak ion flow perturbation being on the order of only $0.1v_A$. In comparison, the peak initial magnitudes of the $U_y$ drifts in the current layer are $0.6v_A$ for the electrons and $0.4v_A$ for the ions. The electric fields $E_x$ and $E_y$ are both strongly modulated by the rippling (Figures 2c and 2d) and both reach maximum magnitudes of $cE/v_AB_0 \approx 2$. The $E_y$ field has nearly equal positive and negative extrema, while the $E_x$ field is negative (directed toward the magnetosheath) almost everywhere in the rippling region. This average negative $E_x$ field serves to shield the low density magnetosphere from ion inflows from the magnetosheath [*Pritchett*, 2008].

[8] Figure 3 shows a stack plot of the evolution of the $E_y$ field at $x = 1.5$ and $z = 0$ over the time interval $32 \leq \Omega_{i0}t \leq 40$. It is clear that the rippling structure is nearly stationary, with only a small drift $U_y \approx 0.06\ v_A$ in the positive $y$ direction (the direction of the initial electron drift). At later times when reconnection becomes appreciable (see section 3.2), the rippling drift speed increases to $U_y \approx 0.2\ v_A$.

[9] Many of the features of the present rippling modes are similar to those of a ballooning/interchange mode in a magnetotail configuration that was identified [*Pritchett and Coroniti*, 2010] as being the low-frequency extension of the lower hybrid drift instability (LHDI) that occurs in straight magnetic field geometry. This tail mode was excited in a 2-D current sheet with reversing field $B_{0x}(x, z)$ in a region of adiabatic electrons and gradients (with opposite sign) for the

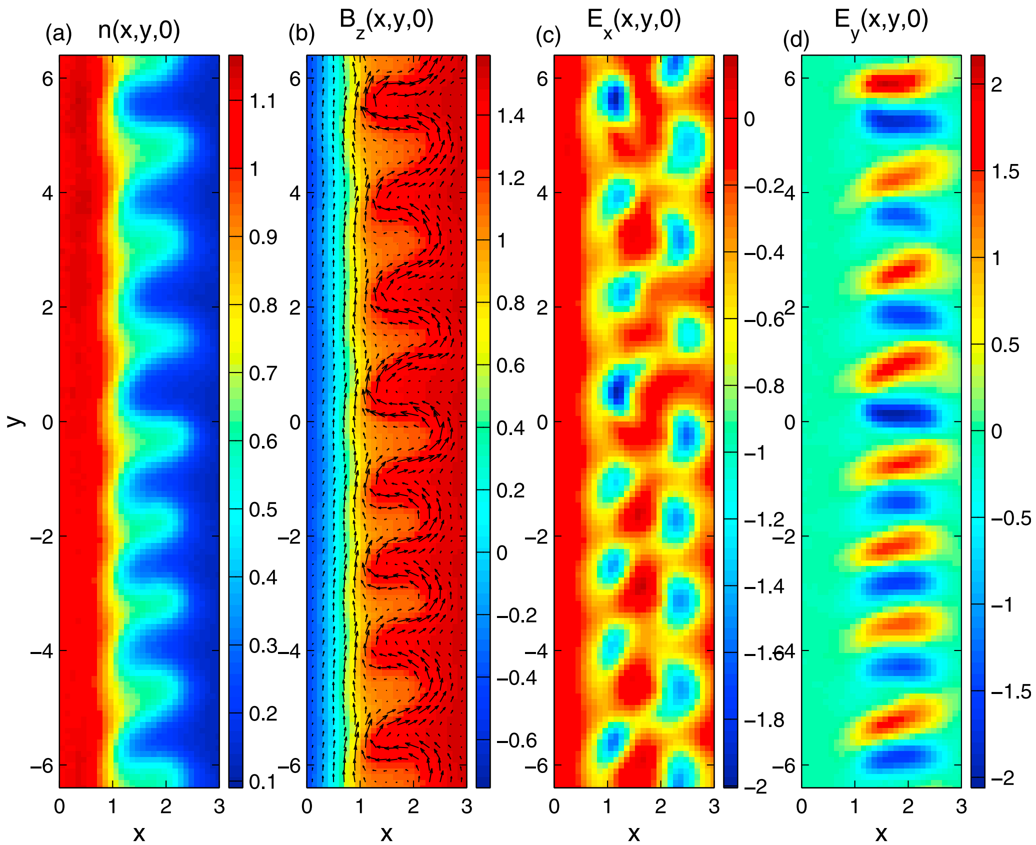


**Figure 2.** Structure in the equatorial plane ($z = 0$) at time $\Omega_{i0}t = 40$ for (a) the density $n/n_0$, (b) the magnetic field $B_z/B_0$ (with the electron flow velocities superimposed as black arrows), (c) the electric field $cE_x/v_AB_0$, and (d) the electric field $cE_y/v_AB_0$.

normal field $B_z$ and density. This is basically the same configuration that occurs on the magnetosphere side of the present 1-D magnetopause current sheet model for $B_{0z}(x)$. The dominant wave number in the magnetotail case was $k_y\rho_i \sim 6$ ($k_y\rho_e \sim 0.7$) compared with the present values of $k_y\rho_i \sim 3.4$ ($k_y\rho_e \sim 0.34$). The magnetotail mode had a mixed character combining features of both ballooning and interchange, with the eigenfunctions extending over long distances along the quasi-parabolic field lines toward the Earth. The present asymmetric current sheet, however, has strictly straight magnetic field lines, and the rippling modes do not exhibit the ballooning/interchange features connected with the presence of an effective gravitational force. Indeed, in many respects they are similar to the low-frequency electromagnetic extension of the LHDI in a symmetric current sheet discussed by *Daughton* [2003]. These latter modes occurred at wavelengths $k_y(\rho_e\rho_i)^{1/2} \sim 1$ intermediate between the electron and ion gyroradius scales. This result is consistent with the value $k_y(\rho_e\rho_i)^{1/2} = 1.1$ for mode 8 in the present simulation. These modes were localized in the center of the (symmetric) current sheet and produced significant modulation of the magnetic field about its initial vanishing value.

[10] Since the development of the present rippling mode occurs well before the influence of the driving field reaches the magnetopause current layer, it seems likely that the

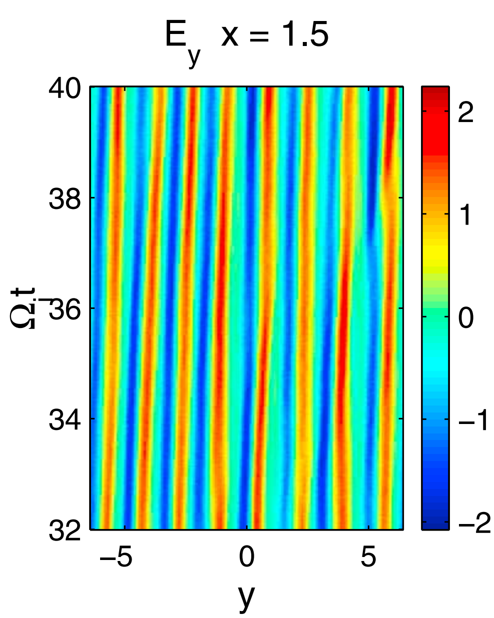


**Figure 3.** Stack plot of the electric field $(c/v_AB_0)E_y(x = 1.5, y, z = 0, t)$ in the equatorial plane over the time interval $32 \leq \Omega_{i0}t \leq 40$.

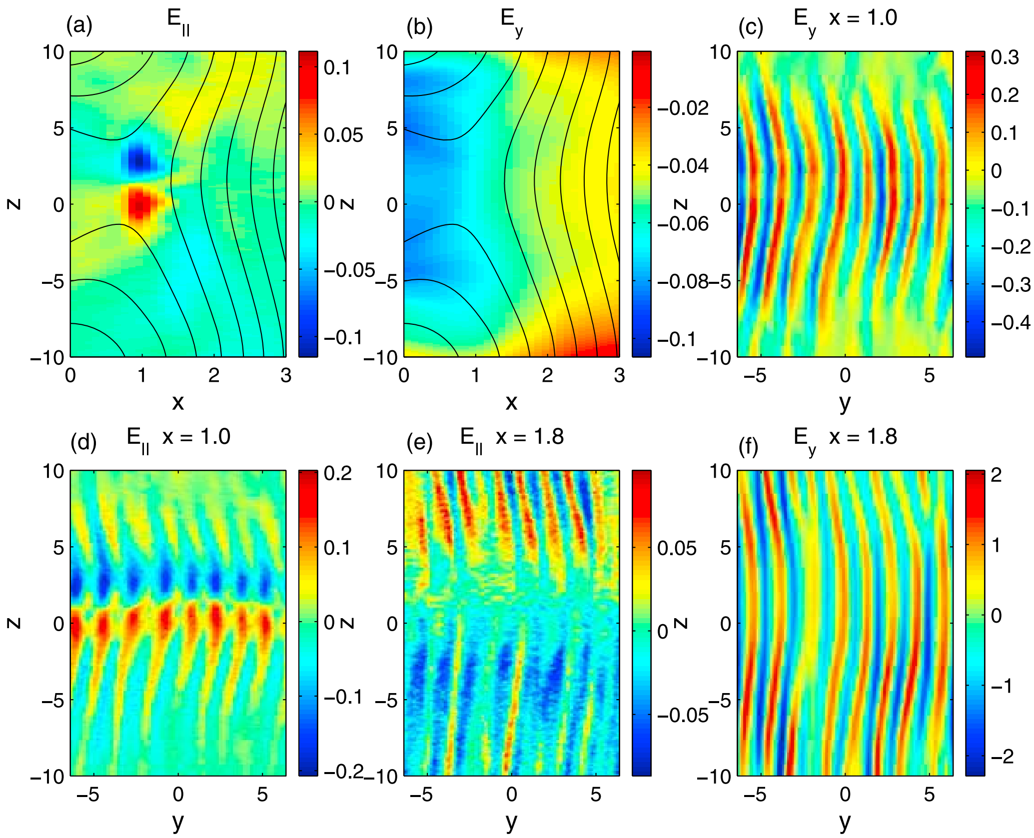


**Figure 4.** Structure of the electric field components $cE_{\|}/v_A B_0$ and $cE_y/v_A B_0$ at time $\Omega_{i0}t = 64$: (a–b) fields plotted in the $x$,$z$ plane averaged over $y$, (c–f) fields plotted in the $y$,$z$ plane at local values of $x/d_i$ = 1.0 and 1.8.

instability represents a spontaneous mode of the asymmetric current layer rather than a response to the external perturbation. This conclusion is strengthened by the results (not shown) of an additional simulation in which the reconnection was initiated by a small seed perturbation rather than by an external driver. Here the rippling mode grew at the same rate and with the same wavelength as in the driven case.

[11] It is also interesting to note that the 3-D simulation shows no clear evidence for the excitation of the usual LHDI [*Krall and Liewer*, 1971; *Davidson and Gladd*, 1975; *Huba et al.*, 1977], which has a much higher frequency and shorter wavelength $k_y\rho_e \sim 1$. In contrast, 2-D simulations in the $x$,$y$ plane with the current asymmetric current sheet configuration do show the presence of a strong LHDI on the low density side. It appears that the presence of finite $k_{\|}$ modes along the strong $B_z$ field in the 3-D case that are absent in the 2-D case prevent the growth of LHDI modes. This is consistent with general theoretical expectations [*Gladd*, 1976] and with 3-D simulation results in a magnetotail configuration [*Pritchett et al.*, 1996] in which an initial finite normal magnetic field component was observed to stabilize LHDI modes.

### 3.2. Effect of Rippling on Reconnection

[12] At times later than $\Omega_{i0}t \sim 40$, the rippling of the current sheet remains well localized in the range $1 < x/d_i < 2.5$, and there is very little reduction in the average gradients of density and magnetic field across the current layer. Once the magnetic field perturbation reaches the center of the system, large-scale reconnection ensues (Figure 1c). Figure 4 shows results for the electric fields $E_{\|}$ and $E_y$ at time $\Omega_{i0}t$ = 64. Figures 4a and 4b show $E_{\|}$ and $E_y$, respectively, in the $x$,$z$ plane averaged over all values of $y$. These are the structures that would be observed in a 2-D $x$,$z$ simulation. There is a localized bipolar $E_{\|}$ field above and below the X line with magnitude $cE_{\|}/v_A B_0 \approx 0.1$ as well as weaker fields with the opposite polarity at larger values of $|z|$ on the magnetosphere side. The average $E_y$ field is relatively structureless with magnitude $cE_y/v_A B_0 \sim 0.07$ near the X line and somewhat smaller on the magnetosphere side. These averages over $y$, however, are quite misleading as to the actual strength of the local fields. Figures 4c–4f show $E_{\|}$ and $E_y$ in the $y$,$z$ plane at $x$ values of 1.0 and 1.8. At both locations $E_{\|}$ and $E_y$ are each strongly modulated by the rippling mode. The local $E_y$ fields are as strong as $cE_y/v_A B_0 \sim 2$, which is some 30 times larger than the $y$ average value. The $E_x$ fields (not shown) are also modulated by the rippling mode, but the contrast with the $y$ average value is not as dramatic due to the net average $E_x$ value in the vicinity of the magnetosphere separatrix. Near the X line ($x = 1.0$), the peak bipolar $E_{\|}$ fields are twice as large as the $y$ average value. The polarity is such that $E_{\|}$ is negative for small positive $z$ and positive for small magnitudes of negative $z$. Such a field structure accelerates electrons away from the X line on both sides of $z$ = 0. For $x \sim 1.8$, the dominant polarity of $E_{\|}$ at large $|z|$ has the opposite sense, so that

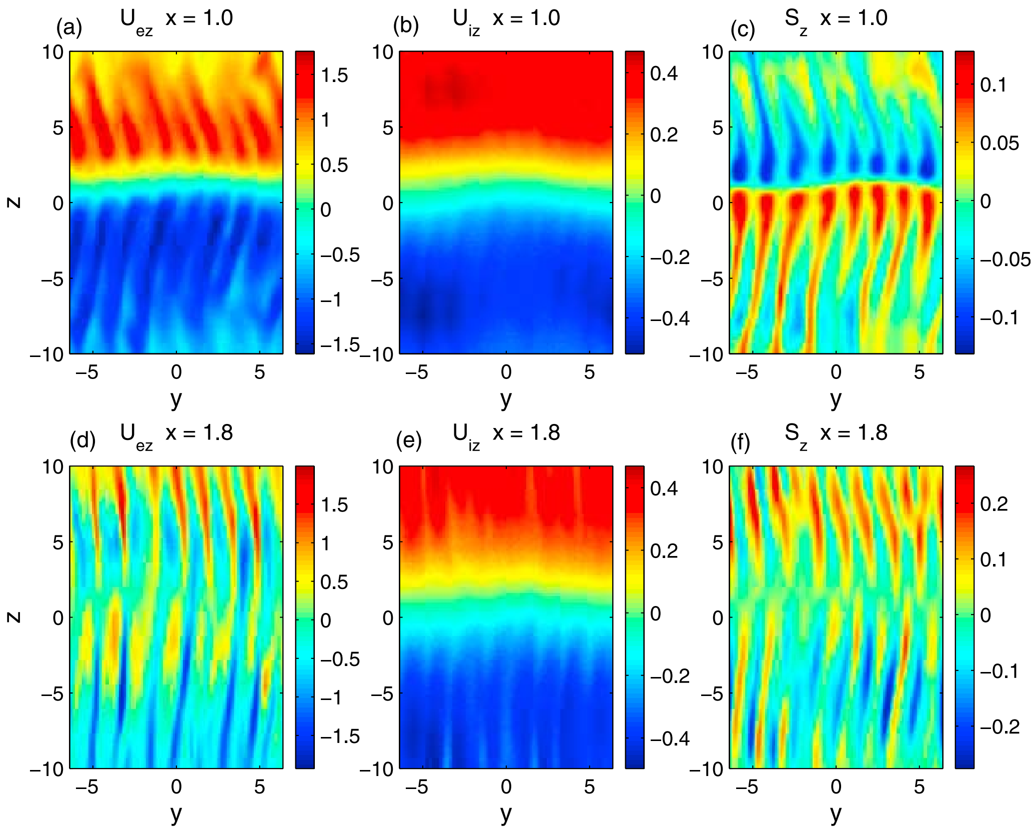


**Figure 5.** Structure at time $\Omega_{i0}t = 64$ in the $y,z$ plane of (a) the electron bulk flow velocity $U_{ez}/v_A$ at $x/d_i = 1.0$, (b) the ion bulk flow velocity $U_{iz}/v_A$ at $x/d_i = 1.0$, (c) the Poynting vector $S_z/v_AB_0^2$ at $x/d_i = 1.0$, (d) the electron bulk flow velocity $U_{ez}/v_A$ at $x/d_i = 1.8$, (e) the ion bulk flow velocity $U_{iz}/v_A$ at $x/d_i = 1.8$, and (f) the Poynting vector $S_z/v_AB_0^2$ at $x/d_i = 1.8$.

electrons tend to be accelerated back toward $z = 0$. At some values of $y$, however, the opposite sign of $E_\parallel$ is present.

[13] The rippling mode also produces a modulation in the reconnection outflow $U_{ez}$ and the Poynting vector component $S_z$ as shown in Figure 5. The electron flows near the X line (Figure 5a) show that the electrons are accelerated to speeds ~1.5 $v_A$ in a distance of the order of $d_i$ by the $E_\parallel$ field. The fact that the maximum electron speeds are displaced in the negative $y$ direction as $|z|$ increases indicates that the accelerating structures are traveling in the positive $y$ direction (eastward), consistent with the observed motion of the rippling mode. The ion modulation near the X line (Figure 5b) is much less pronounced. At $x = 1.8$ the electron flows (Figure 5d) show interlaced motions toward and away from the mid plane. The ion outflows at $x = 1.8$ (Figure 5e) show a weak modulation due to the rippling mode. The Poynting vector $S_z$ exhibits a similar change in structure between $x = 1.0$ (Figure 5c) and $x = 1.8$ (Figure 5f). At the former location, the Poynting flux is toward the X line and arises predominantly from the $E_xB_y$ contribution. At the latter position, the flux is predominantly away from the center of the current sheet and arises mainly from the $-E_yB_x$ term. Note that neither of these Poynting vector configurations (at $x = 1.0$ and 1.8) are consistent with the Alfvén edge described by *Vaivads et al.* [2010]. At the former the Poynting flux is directed in toward the X line consistent with the $E_x \times B_y$ direction associated with the self-consistently generated Hall field $B_y$, while the latter (which is located outside the separatrix) depends on the rippling $E_y$ field to drive the Poynting outflow.

## 4. Discussion

[14] Since the present simulation has an unrealistic value of $m_i/m_e = 50$ for the ion to electron mass ratio, there is some question as to the proper choice of extrapolation procedure to effect a comparison between the simulation results and observations. It is by now well established, both from general scaling arguments based on conservation laws applied across the dissipation region [*Cassak and Shay*, 2007] and by explicit studies in which $m_i/m_e$ is varied in PIC simulations [*Shay and Drake*, 1998; *Hesse et al.*, 1999; *Pritchett*, 2001; *Ricci et al.*, 2002; *Shay et al.*, 2007; *Pritchett*, 2010], that the reconnection electric field scales as $v_AB_0$, and we shall employ this scaling. For length and time scales, the situation is not as clear. The rippling mode clearly occurs on ion scales, but in the absence of a detailed kinetic theory for the mode, it is uncertain whether the ion inertia length or ion gyroradius is the more appropriate parameter. We will scale the results using the former as well as the Alfvén transit time across the inertia length.

[15] For typical subsolar magnetopause values [e.g., *Mozer and Pritchett*, 2010] of magnetosheath density $n_0$ = 3 cm$^{-3}$ and average magnitude $B_0$ of the magnetosheath and magnetosphere magnetic fields $B_0$ = 60 nT, the ion inertia length $d_i$ = 130 km, the Alfvén speed $v_A$ = 750 km/s, and the

reference electric field $v_A B_0$ = 45 mV/m. The peak values of the local perpendicular electric fields observed in the simulation are thus ~90 mV/m, which is quite compatible with the recent Polar data [*Mozer and Pritchett*, 2010]. The simulation parallel electric fields, however, are still much smaller than the observed values. The bipolar $E_{\|}$ structures near the X line are ~10 mV/m, but the fields on the magnetosphere side away from the X line, which are likely the fields encountered by Polar, are at most only a few mV/m. Furthermore, the time duration of the simulation fields is not consistent with the Polar observations. The wavelength of the rippled current sheet in the simulation is $1.6d_i$ or 210 km. The drift speed of the rippled structure is $\sim 0.2v_A$ or ~150 km/s. Thus a pulse of density and electric field would sweep past a satellite in the order of a second, which is at least a factor of 100 times longer than the bursts observed by Polar. Likewise, except for the immediate region of the X line, the simulation does not show a strong correlation between the parallel field structures and density minima.

[16] The 3-D simulations have demonstrated that there can be significant differences in the density and field structure at the subsolar magnetopause as compared to a 2-D treatment. At least in this initial foray into 3-D, however, the changes do not yet produce agreement with the electric field burst observations from the Polar satellite. In particular, it appears that the rippling mode, which mainly is effective on an ion scale, does not produce the large amplitude, few ms electric field bursts that are undoubtedly related to electron dynamics. There are a number of modifications that could be made to the simulations to try to obtain better agreement. One clear possibility is to add an initial guide field component to the magnetic field. Three-dimensional simulations in a symmetric configuration with a very strong guide field $\gg B_0$ and a sub-$d_i$ current sheet thickness [*Drake et al.*, 2003; *Che et al.*, 2009] have observed the formation of electron holes produced by the Buneman instability that were accompanied by intense electric fields [*Cattell et al.*, 2005]. Whether such a process survives with the guide field comparable to or smaller than $B_0$ and in the presence of the magnetopause asymmetries is at present unknown. Another improvement would be to generalize the initial magnetopause equilibrium to include separate magnetosheath and magnetosphere populations with different temperatures. This would introduce an explicit temperature gradient across the magnetopause. The Polar burst observations with large parallel and perpendicular electric fields typically show a temperature ratio $T_i/T_e \sim 10$ and sometimes as large as 30. This reflects the presence of hotter magnetospheric ions. Whether this temperature effect affects the large fields remains to be determined.

[17] **Acknowledgments.** One of us (P.L.P.) would like to thank F. V. Coroniti and W. Daughton for valuable discussions. This research was supported by NASA grants NNX08AM15G, NNG05GL27G, and NNG05GC72G and contract NAS5-02099-07/09. The computations in this work were made possible by allocations of advanced computing resources by the National Science Foundation on Kraken (a Cray XT5) at the National Institute for Computational Sciences (http://www.nics.tennessee.edu) and by the NASA High-End Computing (HEC) Program through the NASA Advanced Supercomputing (NAS) Division at Ames Research Center.

[18] Philippa Browning thanks the reviewers for their assistance in evaluating this manuscript.

## References

Birn, J., and E. R. Priest (Eds.) (2007), *Reconnection of Magnetic Fields: Magnetohydrodynamics and Collisionless Theory and Observations*, chapter 3, Cambridge Univ. Press, Cambridge, U. K.

Büchner, J., and L. M. Zelenyi (1987), Chaotization of the electron motion as the cause of an internal magnetotail instability and substorm onset, *J. Geophys. Res.*, *92*, 13,456.

Cassak, P. A., and M. A. Shay (2007), Scaling of asymmetric magnetic reconnection: General theory and collisional simulations, *Phys. Plasmas*, *14*, 102114.

Cattell, C., et al. (2005), Cluster observations of electron holes in association with magnetotail reconnection and comparison to simulations, *J. Geophys. Res.*, *110*, A01211, doi:10.1029/2004JA010519.

Che, H., J. F. Drake, M. Swisdak, and P. H. Yoon (2009), Nonlinear development of streaming instabilities in strongly magnetized plasma, *Phys. Rev. Lett.*, *102*, 145004, doi:10.1103/PhysRevLett.102.145004.

Daughton, W. (2003), Electromagnetic properties of the lower-hybrid drift instability in a thin current sheet, *Phys. Plasmas*, *10*, 3103.

Daughton, W., and H. Karimabadi (2005), Kinetic theory of collisionless tearing at the magnetopause, *J. Geophys. Res.*, *110*, A03217, doi:10.1029/2004JA010751.

Davidson, R. C., and N. T. Gladd (1975), Anomalous transport properties associated with the lower-hybrid-drift instability, *Phys. Fluids*, *18*, 1327.

Drake, J. F., M. Swisdak, C. Cattell, M. A. Shay, B. N. Rogers, and A. Zeiler (2003), Formation of electron holes and particle energization during magnetic reconnection, *Science*, *299*, 873.

Ding, D. Q., L. C. Lee, and D. W. Swift (1992), Particle simulations of driven collisionless magnetic reconnection at the dayside magnetopause, *J. Geophys. Res.*, *97*, 8453.

Galeev, A. A., M. M. Kuznetsova, and L. M. Zelenyi (1986), Magnetopause stability threshold for patchy reconnection, *Space Sci. Rev.*, *44*, 1.

Gladd, N. T. (1976), The lower hybrid drift instability and the modified two stream instability in high density theta pinch environments, *Plasma Phys.*, *18*, 27.

Hesse, M., K. Schindler, J. Birn, and M. Kuznetsova (1999), The diffusion region in collisionless magnetic reconnection, *Phys. Plasmas*, *6*, 1781.

Huang, J., Z. W. Ma, and D. Li (2008), Debye-length scaled structure of perpendicular electric field in collisionless magnetic reconnection, *Geophys. Res. Lett.*, *35*, L10105, doi:10.1029/2008GL033751.

Huba, J. D., N. T. Gladd, and K. Papadopoulos (1977), The lower-hybrid-drift instability as a source of anomalous resistivity for magnetic field line reconnection, *Geophys. Res. Lett.*, *4*, 125.

Krall, N. A., and P. C. Liewer (1971), Low frequency instabilities in magnetic pulses, *Phys. Rev. A*, *4*, 2094.

Mozer, F. S., and P. L. Pritchett (2009), Regions associated with electron physics in asymmetric magnetic field reconnection, *Geophys. Res. Lett.*, *36*, L07102, doi:10.1029/2009GL037463.

Mozer, F. S., and P. L. Pritchett (2010), Spatial, temporal, and amplitude characteristics of parallel electric fields associated with subsolar magnetic field reconnection, *J. Geophys. Res.*, *115*, A04220, doi:10.1029/2009JA014718.

Mozer, F. S., and A. Retinò (2007), Quantitative estimates of magnetic field reconnection properties from electric and magnetic field measurements, *J. Geophys. Res.*, *112*, A10206, doi:10.1029/2007JA012406.

Mozer, F. S., S. D. Bale, and T. D. Phan (2002), Evidence of diffusion regions at a subsolar magnetopause crossing, *Phys. Rev. Lett.*, *89*, 015002.

Mozer, F. S., P. L. Pritchett, J. Bonnell, D. Sundkvist, and M. T. Chang (2008), Observations and simulations of asymmetric magnetic field reconnection, *J. Geophys. Res.*, *113*, A00C03, doi:10.1029/2008JA013535.

Pritchett, P. L. (2001), Geospace Environment Modeling magnetic reconnection challenge: Simulations with a full particle electromagnetic code, *J. Geophys. Res.*, *106*, 3783, doi:10.1029/1999JA001006.

Pritchett, P. L. (2008), Collisionless magnetic reconnection in an asymmetric current sheet, *J. Geophys. Res.*, *113*, A06210, doi:10.1029/2007JA012930.

Pritchett, P. L. (2010), Onset of magnetic reconnection in the presence of a normal magnetic field: Realistic ion to electron mass ratio, *J. Geophys. Res.*, *115*, A10208, doi:10.1029/2010JA015371.

Pritchett, P. L., and F. V. Coroniti (2010), A kinetic ballooning/interchange instability in the magnetotail, *J. Geophys. Res.*, *115*, A06301, doi:10.1029/2009JA014752.

Pritchett, P. L., and F. S. Mozer (2009), Asymmetric magnetic reconnection in the presence of a guide field, *J. Geophys. Res.*, *114*, A11210, doi:10.1029/2009JA014343.

Pritchett, P. L., F. V. Coroniti, and V. K. Decyk (1996), Three-dimensional stability of thin quasi-neutral current sheets, *J. Geophys. Res.*, *101*, 27,413.

Ricci, P., G. Lapenta, and J. U. Brackbill (2002), GEM reconnection challenge: Implicit kinetic simulations with the physical mass ratio, *Geophys. Res. Lett.*, *29*(23), 2088, doi:10.1029/2002GL015314.
Shay, M. A., and J. F. Drake (1998), The role of electron dissipation on the rate of collisionless magnetic reconnection, *Geophys. Res. Lett.*, *25*, 3759.
Shay, M. A., J. F. Drake, and M. Swisdak (2007), Two-scale structure of the electron dissipation region during collisionless magnetic reconnection, *Phys. Rev. Lett.*, *99*, 155002.
Swisdak, M., B. N. Rogers, J. F. Drake, and M. A. Shay (2003), Diamagnetic suppression of component magnetic reconnection at the magnetopause, *J. Geophys. Res.*, *108*(A5), 1218, doi:10.1029/2002JA009726.
Tanaka, K. G., et al. (2008), Effects on magnetic reconnection of a density asymmetry across the current sheet, *Ann. Geophys.*, *26*, 2471.
Vaivads, A., A. Retinò, Yu. V. Khotyaintsev, and M André (2010), The Alfvén edge in asymmetric reconnection, *Ann. Geophys.*, *28*, 1327, doi:10.5194/angeo-2813272010.

F. S. Mozer, Space Sciences Laboratory, University of California, Berkeley, CA 94720, USA. (fmozer@ssl.berkeley.edu)
P. L. Pritchett, Department of Physics and Astronomy, University of California, 405 Hilgard Ave., Los Angeles, CA 90095-1547, USA. (pritchet@physics.ucla.edu)